



Non-invasive manipulation scheme of spherical particle in viscous fluids in a tube based on acoustic radiation force

Menyang Gong,¹  Xin Xu,¹ Zhonghan Fei,¹ Yuanyuan Li,¹ Teng Liu,¹ Shenlian Gao,¹ Jiehui Liu,¹ Aijun He,² and Xiaozhou Liu^{1,a)} 

¹Key Laboratory of Modern Acoustics, Institute of Acoustics and School of Physics, Collaborative Innovation Center of Advanced Microstructures, Nanjing University, Nanjing 210093, China

²School of Electronic Science and Engineering, Nanjing University, Nanjing 210023, China

ABSTRACT:

A theoretical solution of the acoustic radiation force (ARF) on spherical particles by an arbitrary beam in viscous fluids in a tube is proposed. Based on the parametric design with the purpose of promoting calculi in the urinary system, theoretical solutions and finite element simulations are carried out, which mutually confirm the accuracy and feasibility of the scheme. The variation law of the ARF with adjustable parameters, such as incident angle, frequency spectrum, particle radius, tube radius, and viscosity, is studied, and the mechanism of the variation law is explained. This solution lays a foundation for the application of non-contact and non-invasive in-tube manipulation based on ARF in medicine and life sciences. © 2023 Acoustical Society of America.

<https://doi.org/10.1121/10.0017113>

(Received 3 November 2022; revised 15 January 2023; accepted 15 January 2023; published online 2 February 2023)

[Editor: Mark F. Hamilton]

Pages: 812–820

I. INTRODUCTION

Since the optical tweezers won the Nobel Prize,¹ how to construct potential wells through the design of beams and structures for non-contact manipulation has become a research hotspot.^{2–4} The acoustic radiation force (ARF) is an important nonlinear effect of sound beams. The acoustic tweezers constructed based on the ARF avoid the thermal effect of optical tweezers and have better penetration and biological adaptability.^{5,6} Under free boundary conditions, the ARF of various beams, such as plane wave, Gaussian wave, and Bessel wave, acting on standard particles in ideal fluids has been extensively calculated and discussed.^{7–19} The ARF on particles in viscous fluids with free boundaries has recently been studied.²⁰ Negative ARF solutions based on undiffracted beam designs have also recently been proposed.^{21–24} In the application requirements of industry and life science, the tube line is a common boundary condition, but the ARF on the particles in the tube line environment is rarely studied. Shi *et al.*²⁵ calculated the ARF of spherical particles under a cylindrical boundary in an ideal fluid. However, in practical scenarios, the viscosity of fluids in most tubes cannot be ignored, but in many practical applications, particle manipulation cannot be performed by providing a pressure differential across the tube. In addition, it is even often impossible to place the sound source in the tube. The sound source can only be placed outside the tube to emit sound waves; otherwise, the principle of non-invasiveness and non-contact is violated. In the life sciences, acoustic

tweezers have been proposed to be a meaningful non-contact solution for particle manipulation.^{26–29} For instance, nephrolithiasis is a common disease in urinary system lesions. There are currently four main treatment methods for kidney calculus: drugs for small calculus, extracorporeal shock wave lithotripsy for large calculus, soft mirror non-invasive surgery, and percutaneous nephroscopy with puncture from the kidney minimally invasive surgery. Most of these methods involve contact and have some disadvantages. The source of pain in a considerable number of patients is that the calculus in the ureter cannot be discharged. Invasive surgery may cause great pain to patients. In comparison, non-contact manipulation based on ARF provides a humane and pain-reducing treatment scheme. Therefore, it is of great significance to propose a solution in which the particles in the tube are subjected to the ARF exerted by the sound source outside the tube, which has broad prospects in life science and industrial applications.

II. ANALYSIS OF SOUND FIELD AND THEORETICAL CALCULATION OF ARF

Due to the in-tube environment, most application scenarios require particles to move along the tube, such as the potential need to assist in the discharge of urinary calculi. The scale of the particles is on the same order of magnitude as the inner diameter of the tube. It is worth mentioning that if the scale of the particle is much smaller than the inner diameter of the tube, its influence on the sound field in the tube is small. The coupling effect between the particle and the tube does not need to be considered. The model is, therefore, built as shown in Fig. 1. The outermost layer is the environmental medium. The tube contains a viscous fluid.

^{a)}Also at: State Key Laboratory of Acoustics, Institute of Acoustics, Chinese Academy of Sciences, Beijing 100190, China. Electronic mail: xzliu@nju.edu.cn

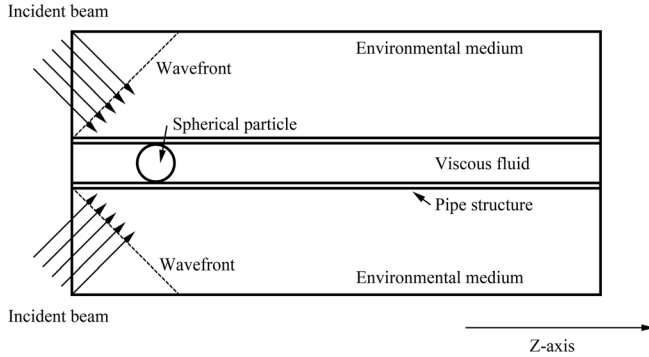


FIG. 1. Sectional view of spherical particle manipulation in a tube based on ARF.

The incoming beam is angled from the left side of the picture. The incident surface of the incident beam is a conical plane. The controlled particles are placed inside the tube, in the irradiated area of the incident beam, based on the consideration of manipulation efficiency. The entire model is rotationally symmetric.

Since the nonlinear effects appear most obvious when the size of the particles is close to the scale of the wavelength, the peak of the ARF often appears in this range. Since they have been set before, the scale of the particles and the inner diameter of the tube are on the same order of magnitude. Therefore, the heat wave propagation mode and the rotational wave propagation mode only need to be considered in the boundary layer, and the mode splitting of the viscous fluid in the tube could just be carried out in the boundary layer. Set the outer radius of the tube as R' and the inner radius as R . The radius of the spherical urinary calculi is a . Since the spectrum above the cutoff frequency has little effect on the ARF, only the contribution of the (0,0) order propagation mode needs to be considered when calculating the ARF on the particles in the tube. The propagation modes refer to the propagation mode in which the variables are separated when solving the sound pressure equation in the tube. The (0,0) propagation mode is a plane wave propagating along the z axis in the tube, and the subscript parameter that needs to take an integer of the cylindrical Bessel function is 0. For the part of the spectrum above the cutoff frequency, the transmission of this part of the momentum by the tube attenuates severely with distance, so the transmission of this part of the momentum can be ignored in the calculation of the ARF in a stable tube. For the efficiency of manipulation, the actual selected incident frequencies will also be mainly distributed in the range of the (0,0) order propagation mode. The frequency of the incident sound wave is below the cutoff frequency of the tube,

$$R < 1.84 \frac{c_0}{\omega}. \quad (1)$$

Here, c_0 is the longitudinal wave number of the viscous fluid in the tube, and ω is the circular frequency of the longitudinal wave in the tube. The frequency of the incident acoustic wave is high, so that the diameter R of the tube is much larger than the thickness of the boundary layer,

$$R \gg \max(d_\mu, d_\kappa). \quad (2)$$

Here, the two limiting factors of the boundary layer are

$$d_\mu = \sqrt{\frac{2\mu}{\omega\rho_0}}, \quad (3a)$$

$$d_\kappa = \sqrt{\frac{2\kappa}{\omega\rho_0 c_{P_0}}}. \quad (3b)$$

Here, μ , κ , ρ_0 , and c_{P_0} are shear modulus, heat capacity ratio, density, and isobaric heat capacity individually.

Since the Laplace operator satisfies the superposition principle, only single-frequency beams need to be considered to cover all situations. It is only necessary to perform spectrum expansion to examine plane waves, so set the incident sound pressure ($R' < r < d + R'$),

$$p_a(\rho, r, \theta) = p_a(r, \theta)e^{ik_z z \cos \phi}. \quad (4)$$

Here, ϕ is the angle between the incident sound beam and the z axis of the cylindrical coordinate system. This phase control essentially simulates the oblique incidence of the beam by manipulating the wavefront. There are also scattered sound waves in the external medium, which are emitted from the tube wall to the surrounding medium, so the velocity potential in the external medium can be expressed as ($r > R'$)

$$\Phi_{out}(r, \theta) = \sum_{n=0}^{\infty} [I_n(2n+1)i^n j_n(k_z r) + D_n h_n^{(1)}(k_z r)] P_n(\cos \theta). \quad (5)$$

Among them, I_n is the known parameter related to the incident wave, and D_n is the undetermined scattering parameter. $h_n^{(1)}$ is Hankle function of the first kind. j_n is spherical Bessel function. The longitudinal wave and transverse velocity potential in the tube wall can be expressed as two parts of convergence and divergence ($R < r < R'$),

$$\Phi_1(r, \theta) = \sum_{n=0}^{\infty} [E_n h_n^{(1)}(k_{1L} r) + F_n j_n(k_{1L} r)] P_n(\cos \theta), \quad (6a)$$

$$\Psi_1(r, \theta) = \sum_{n=0}^{\infty} [E'_n h_n^{(1)}(k_{1L} r) + F'_n j_n(k_{1L} r)] \frac{dP_n(\cos \theta)}{d\theta}. \quad (6b)$$

Similarly, the velocity potential in a viscous fluid in a tube can be expressed as ($r < R$)

$$\Phi_2(r, \theta) = \sum_{n=0}^{\infty} [L_n h_n^{(1)}(k'_z r) + M_n j_n(k'_z r)] P_n(\cos \theta). \quad (7)$$

The velocity potential inside the target elastic spherical particle can be expressed as

$$\Phi_3(r, \theta) = \sum_{n=0}^{\infty} (2n+1) i^n \left[G_n h_n^{(1)}(k_{2L} r) + H_n j_n(k_{2L} r) \right] P_n(\cos \theta), \quad (8a)$$

$$\Psi_3(r, \theta) = \sum_{n=0}^{\infty} (2n+1) i^n \left[G'_n h_n^{(1)}(k_{2t} r) + H'_n j_n(k_{2t} r) \right] \frac{dP_n(\cos \theta)}{d\theta}. \quad (8b)$$

Here, $E_n, F_n, E'_n, F'_n, L_n, M_n, G_n, H_n, G'_n$, and H'_n are undetermined scattering parameters, which are uniquely determined by the boundary condition equations. k_L and k_t are the longitudinal wave number and shear wave number in elastic medium, respectively. It should be mentioned that in addition to the acoustic propagation mode, there are heat waves and rotational waves at the boundary layer, which will be discussed in detail in the processing of boundary conditions.

There are three boundaries in the sound field, namely, the boundary between the external medium and the tube wall, the boundary between the tube wall and the viscous fluid in the tube, and the boundary between the viscous fluid and the controlled target particle. For the boundary between the external medium and the tube wall ($z < d \cot \theta$),

$$v_{out r}|_{r=R'} = v_{1r}|_{r=R'}, \quad (9a)$$

$$v_{out \theta}|_{r=R'} = v_{1\theta}|_{r=R'}, \quad (9b)$$

$$\sigma_{out rr}|_{r=R'} = \sigma_{1rr}|_{r=R'}, \quad (9c)$$

$$\sigma_{out r\theta}|_{r=R'} = \sigma_{1r\theta}|_{r=R'}. \quad (9d)$$

Here, v_{out} represents the velocity of the external medium, and σ_{out} represents the stress of the external medium. The left sides of the equations are the parameters of the external medium, and the right sides are the parameters of the tube wall medium. Due to the symmetry of the model, the momentum transfer in the direction perpendicular to the z axis does not contribute to the ARF, so the calculation of the ARF actually only needs to consider the components in the direction parallel to the z axis. The specific expression of continuity boundary condition is

$$v_{out r} = \frac{\partial \Phi_{out}}{\partial r}, \quad (10a)$$

$$v_{1r} = \frac{\partial \Phi_1}{\partial r} + \frac{1}{r \sin \theta} \frac{\Psi_1 \sin \theta}{\partial \theta}, \quad (10b)$$

$$v_{out \theta} = \frac{1}{r} \frac{\partial \Phi_{out}}{\partial \theta}, \quad (10c)$$

$$v_{1\theta} = \frac{1}{r} \frac{\partial \Phi_1}{\partial \theta} - \frac{1}{r} \frac{\partial (r \Psi_1)}{\partial r}, \quad (10d)$$

$$\sigma_{out rr} = -\lambda k_z^2 \Phi_{out} + 2\mu \left\{ \frac{\partial^2}{\partial r^2} \Phi_{out} \right\}, \quad (10e)$$

$$\sigma_{1rr} = -\lambda k_{1L}^2 \Phi_1 + 2\mu \left\{ \frac{\partial^2}{\partial r^2} \left[\Phi_1 + \frac{\partial}{\partial r} (r \Psi_1) \right] + k_{1t}^2 (r \Psi_1) \right\}, \quad (10f)$$

$$\sigma_{out r\theta} = \mu \left\{ 2 \frac{\partial}{\partial r} \left[\frac{1}{r} \frac{\partial}{\partial \theta} \Phi_{out} \right] \right\}, \quad (10g)$$

$$\sigma_{1r\theta} = \mu \left\{ 2 \frac{\partial}{\partial r} \left[\frac{1}{r} \frac{\partial}{\partial \theta} \left[\Phi_1 + \frac{\partial}{\partial r} (r \Psi_1) \right] \right] + k_{1t}^2 \frac{\partial \Psi_1}{\partial \theta} \right\}. \quad (10h)$$

For the boundary between the tube wall and the viscous fluid in the tube ($z < d \cot \theta$),

$$v_{1r}|_{r=R} = v_{2r}|_{r=R}, \quad (11a)$$

$$v_{1\theta}|_{r=R} = v_{2\theta}|_{r=R}, \quad (11b)$$

$$\sigma_{1rr}|_{r=R} = \sigma_{2rr}|_{r=R}, \quad (11c)$$

$$\sigma_{1r\theta}|_{r=R} = \sigma_{2r\theta}|_{r=R}. \quad (11d)$$

The specific expression of continuity boundary condition is

$$v_{1r} = \frac{\partial \Phi_1}{\partial r}, \quad (12a)$$

$$v_{1\theta} = \frac{1}{r} \frac{\partial \Phi_1}{\partial \theta}, \quad (12b)$$

$$\sigma_{1rr} = -\lambda k_L^2 \Phi_1 + 2\mu \left\{ \frac{\partial^2}{\partial r^2} \Phi_1 \right\}, \quad (12c)$$

$$\sigma_{1r\theta} = \mu \left\{ 2 \frac{\partial}{\partial r} \left[\frac{1}{r} \frac{\partial}{\partial \theta} \Phi_1 \right] \right\}. \quad (12d)$$

Here, γ is the ratio of constant pressure heat capacity to constant volume heat capacity. Propagation of sound beams in tubes containing viscous fluids requires consideration of boundary layer effects,

$$T_2(R, \theta) \approx \frac{(\gamma - 1) p_{a0}}{\rho_0 c_0^2 \beta_{P_0}} + T_{h0} = 0, \quad (13a)$$

$$v_{2\rho}(R, \theta) \approx i k_{ar} \frac{p_{a0}}{\theta \rho_0} \cdot \frac{J_1(k_{ar} R)}{J_0(k_{ar} R)} - i k_{hr} l_{\kappa} c_0 \beta_{P_0} T_{h0} + v_{\mu \rho_0} = v_{1r}(R, \theta), \quad (13b)$$

$$v_{2z}(R, \theta) \approx k'_z \frac{p_{a0}}{\theta \rho_0} + i k'_z l_{\kappa} c_0 \beta_{P_0} T_{h0} + \frac{k_{\mu \rho}}{k'_z} v_{\mu \rho_0} = v_{1z}(R, \theta). \quad (13c)$$

The temperature continuous boundary condition can actually be solved directly for dimensionality reduction,

$$T_{h0} = -\frac{(\gamma - 1) p_{a0}}{\rho_0 c_0^2 \beta_{P_0}}. \quad (14)$$

Substituting the temperature expression into the velocity continuum has

$$i k_{ar} \frac{p_{a0}}{\omega \rho_0} \cdot \frac{J_1(k_{ar} R)}{J_0(k_{ar} R)} + i k_{hr} l_{\kappa} c_0 \beta_{P_0} \frac{(\gamma - 1) p_{a0}}{\rho_0 c_0^2 \beta_{P_0}} + v_{\mu \rho_0} = v_{1\rho}(R, \omega), \quad (15a)$$

$$k_z \frac{p_{a0}}{\omega \rho_0} - i k_z l_{\kappa} c_0 \beta_{P_0} \frac{(\gamma - 1) p_{a0}}{\rho_0 c_0^2 \beta_{P_0}} + \frac{k_{\mu \rho}}{k_z} v_{\mu \rho_0} = v_{1z}(R, \omega). \quad (15b)$$

Since the diameter of the tube is much larger than the convention of the boundary layer, the Bessel function can be approximated by small quantities,

$$\frac{k_{ar}}{k_0 \rho_0 c_0} \cdot \frac{J_1(k_{ar} R)}{J_0(k_{ar} R)} \approx \frac{k_{ar}^2 R}{2 k_0 \rho_0 c_0}. \quad (16)$$

Combining the above equations, we can know that the sound beam in the tube is actually attenuated,

$$k'_z \approx \frac{\omega}{c_0} \left\{ 1 + \sqrt{\frac{1}{2k_0}} \frac{1}{R} \left[\sqrt{l_\mu} + \sqrt{l_\kappa}(\gamma - 1) \right] \right\} + i \left\{ \sqrt{\frac{1}{2k_0}} \frac{1}{R} \left[\sqrt{l_\mu} + \sqrt{l_\kappa}(\gamma - 1) \right] \right\}, \quad (17a)$$

$$l_\mu = \sqrt{\frac{\mu}{\omega \rho_0}}, \quad (17b)$$

$$l_\kappa = \sqrt{\frac{\kappa}{\omega \rho_0 c_{p0}}}. \quad (17c)$$

The boundary conditions for the viscous fluid and the controlled target particles are

$$v_{2r}|_{r=a} = v_{3r}|_{r=a}, \quad (18a)$$

$$v_{2\theta}|_{r=a} = v_{3\theta}|_{r=a}, \quad (18b)$$

$$\sigma_{2rr}|_{r=a} = \sigma_{3rr}|_{r=a}, \quad (18c)$$

$$\sigma_{2r\theta}|_{r=a} = \sigma_{3r\theta}|_{r=a}. \quad (18d)$$

Here, the expansions are

$$v_{3r} = \frac{\partial \Phi_3}{\partial r} + \frac{1}{r \sin \theta} \frac{\Psi_3 \sin \theta}{\partial \theta}, \quad (19a)$$

$$v_{3\theta} = \frac{1}{r} \frac{\partial \Phi_3}{\partial \theta} - \frac{1}{r} \frac{\partial (r \Psi_3)}{\partial r}, \quad (19b)$$

$$\sigma_{3rr} = -\lambda k_{3L}^2 \Phi_3 + 2\mu \left\{ \frac{\partial^2}{\partial r^2} \left[\Phi_3 + \frac{\partial}{\partial r} (r \Psi_3) \right] + k_{3t}^2 (r \Psi_3) \right\}, \quad (19c)$$

$$\sigma_{3r\theta} = \mu \left\{ 2 \frac{\partial}{\partial r} \left[\frac{1}{r} \frac{\partial}{\partial \theta} \left[\Phi_3 + \frac{\partial}{\partial r} (r \Psi_3) \right] \right] + k_{3t}^2 \frac{\partial \Psi_3}{\partial \theta} \right\}. \quad (19d)$$

Here, k_L and k_t are the wavenumbers of longitudinal and transverse waves inside the controlled spherical particle, respectively. The scattering coefficients of spherical particles can be organized in matrix form,

$$\begin{bmatrix} a_{rn} & b_{rn} & a'_{rn} & b'_{rn} \\ a_{tn} & b_{tn} & a'_{tn} & b'_{tn} \\ A_{rn} & B_{rn} & A'_{rn} & B'_{rn} \\ A_{tn} & B_{tn} & A'_{tn} & B'_{tn} \end{bmatrix} \begin{bmatrix} A_n \\ B_n \\ A'_n \\ B'_n \end{bmatrix} = \begin{bmatrix} c_{rn} \\ c_{tn} \\ C_{rn} \\ C_{tn} \end{bmatrix}. \quad (20)$$

The specific parameters of the scattering matrix are listed in the [Appendix](#).

After the velocity potential distribution of the sound field is solved by the undetermined coefficient method, the

ARF can be solved. By definition, the ARF can be obtained by annular integration of the stress tensor at the surface of a spherical particle,

$$\mathbf{F} = \left\langle \iint_{S_0} \boldsymbol{\sigma} d\mathbf{S} \right\rangle. \quad (21)$$

Here, $\langle \rangle$ is the time average, S_0 is the surface of the spherical particle, and $\boldsymbol{\sigma}$ is the stress tensor. In a viscous fluid, the stress tensor satisfies

$$\boldsymbol{\sigma} = (-p_1 + \lambda' \nabla \cdot \mathbf{v}) \mathbf{E} + 2\mu' \mathbf{e}. \quad (22)$$

Here, \mathbf{E} is the unit vector. The deformation rate tensor is

$$\mathbf{e} = \frac{(\nabla \mathbf{v}) + (\nabla \mathbf{v})^T}{2}. \quad (23)$$

Here, λ' is the expansion viscosity coefficient, and μ' is the dynamic viscosity coefficient. The sound pressure p_1 has an expanded expression,

$$p_1 = \rho_0 \left(\frac{\lambda' + 2\mu'}{\rho_0} \Delta - \frac{\partial}{\partial t} \right) \Phi_2 + \frac{\rho_0}{2c_0} \left(\frac{\partial \Phi_2}{\partial t} \right) - \frac{1}{2} \rho_0 (\nabla \Phi_2)^2 - \frac{\lambda' + 2\mu'}{c_0^2} \frac{\partial \Phi_2}{\partial t} \Delta \Phi_2. \quad (24)$$

Thereby, the ARF on spherical particles in the viscous medium in the tube is obtained. The calculation of the ARF can be divided into two steps. The first step is to obtain the sound pressure distribution of the sound field, and the second step is to calculate the ARF through the sound pressure. Generally, only linear acoustics need to be considered in the first step, thus, satisfying the principle of superposition. In the second step, because there is a time-averaged calculation process, the Fourier transform itself is an orthogonal spectrum sequence, so the integrals of cross-terms with different frequencies in the time domain are all zero. Thus, the second step also satisfies the principle of superposition. Therefore, although the ARF is a nonlinear effect, the principle of superposition still works in for a multi-frequency acoustic field. Based on the superposition principle, the ARF of complex incident waves can be obtained by linear superposition of the ARF generated by single-frequency waves obtained from spectral analysis.

III. THEORETICAL SOLUTION AND FINITE ELEMENT SIMULATION

To verify the correctness of the algorithm and the feasibility of this approach, theoretical solutions based on the algorithm proposed in Sec. II and finite element simulations based on COMSOL are carried out. The calculus and ureteral aggregate scales we have chosen in the paper are those of general anatomy. The lumens of the ureter vary in size, with a diameter of about 2–5 mm. There are three physiologically narrow parts and two dilated parts. For physiological stenosis, at the ureteropelvic junction, its diameter is about 2 mm; when it passes through the branch of the common iliac

TABLE I. Parameter selection of interstitial fluid and urine.

Parameter	Symbol	Numerical value
Sound speed of interstitial fluid (environmental medium)	c_{IF}	1580 m/s
Density of interstitial fluid (environmental medium)	ρ_{IF}	$1.054 \times 10^3 \text{ kg/m}^3$
Sound speed of urine (viscous fluid)	c_0	1480 m/s
Density of urine (viscous fluid)	ρ_0	$1.010 \times 10^3 \text{ kg/m}^3$
Shear modulus of urine (viscous fluid)	μ_0	$1.002 \times 10^{-3} \text{ kg/(m}\cdot\text{s)}$
Heat capacity ratio of urine (viscous fluid)	κ_0	$0.597 \text{ W/(s}\cdot\text{K)}$
Dynamic viscosity coefficient of urine (viscous fluid)	μ'	$2.98 \times 10^{-3} \text{ Pa}\cdot\text{s}$
Expansion viscosity coefficient of urine (viscous fluid)	λ'	$2.4 \times 10^{-3} \text{ Pa}\cdot\text{s}$
Isobaric heat capacity of urine (viscous fluid)	c_{P_0}	$4.17 \times 10^3 \text{ J/(kg}\cdot\text{K)}$

TABLE II. Parameter selection of ureter and calcium oxalate.

Parameter	Symbol	Numerical value
The inner radius of ureter (tube structure)	R	0.75 mm
The outer radius of ureter (tube structure)	R'	1 mm
Radius of spherical particles	a	0.74 mm
Density of ureter (tube structure)	ρ_u	$1.1 \times 10^3 \text{ kg/m}^3$
Young's modulus of ureter (tube structure)	E_{ru}	0.3 MPa
Poisson ratio of ureter (tube structure)	ν_u	0.49
Density of calcium oxalate (spherical particle)	ρ_{MO}	$2.2 \times 10^3 \text{ kg/m}^3$
Young's modulus of calcium oxalate (spherical particle)	E_{rMO}	2.65 GPa
Poisson ratio of calcium oxalate (spherical particle)	ν_{MO}	0.41

artery, it is about 3 mm; when it enters the bladder wall, it is about 1–2 mm. The dilation part is in the lumbar segment, its diameter is about 6 mm, and the pelvic segment is about 4 mm. Since the diameter of the urinary system and the scale of the urinary calculi are on the order of millimeters, the parameters are selected as shown in Tables I and II.

Unless otherwise specified, the parameters in Tables I and II are used for subsequent calculations and simulations. The external medium, the medium in the tube, the medium of the tube, and the medium of the spherical particle are interstitial fluid, urine, ureter, and calcium oxalate, individually. Within the allowable error range, the results of theoretical solution and finite element simulation confirm each other, and the validity and accuracy of the algorithm are verified.

A. The relationship between the ARF and the incident spectrum

The angle between the incident beam and the z axis is fixed as $\phi = 45^\circ$. As shown in Fig. 2, the sound pressure level distribution images of the incident sound beam frequencies of 500, 600, 700, 800, 900, 1000, 1100, and 1200 kHz are drawn; it can be seen that the sound field near the spherical particle exhibits obvious asymmetry along the z axis, and the small ball is subjected to obvious ARF. As shown in Fig. 3, the comparison of the ARF on the spherical particles in the tube vs the incident frequency based on theoretical solution and finite element simulation is plotted. Since the scale of the particles is on the order of millimeters, even under the boundary where the reflection of the sound field by the tube wall is relatively severe, the particles can obtain the acceleration on the order of m/s^2 through the momentum transfer of the ARF; for that, the particle mass is about on the order of 10^{-5} kg . This is conducive to promoting the excretion of urinary calculi, which has important application prospects. The black solid line in the figure is the result of the theoretical solution, and the blue diamond point is the result of the finite element simulation.

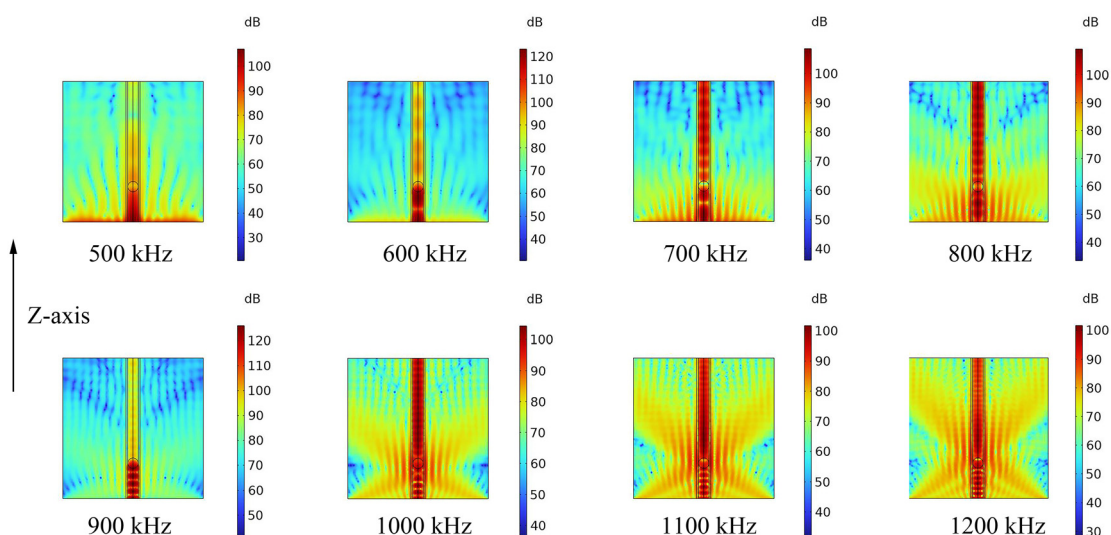


FIG. 2. (Color online) Sectional view of the sound pressure level distribution when the incident frequency is 500, 600, 700, 800, 900, 1000, 1100, and 1200 kHz.

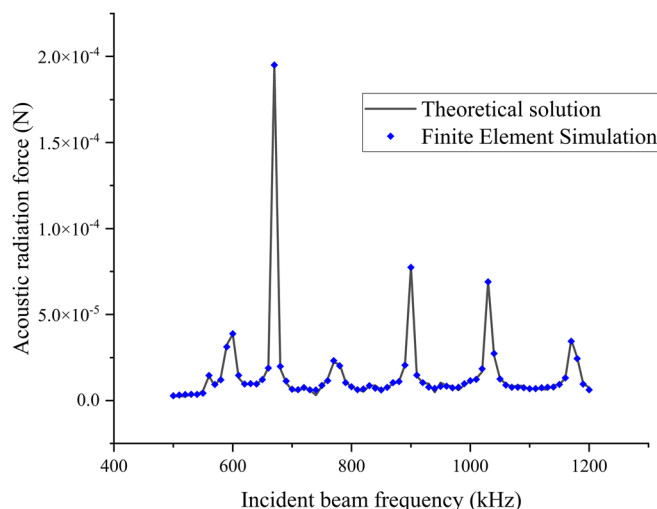


FIG. 3. (Color online) The ARF on the controlled spherical particle changing with the frequency of the incident acoustic beam.

B. The relationship between the ARF and the incident angle

The frequency of the incident beam is fixed as $f = 1$ MHz, and as shown in Fig. 4, the sound pressure level distribution images of the incident sound beam and the z axis at angles of 30° , 45° , and 60° are drawn, and it can be seen that the angle parameter is also an important factor affecting the ARF received by the spherical particle. As shown in Fig. 5, the comparison of the ARF on spherical particles in the tube obtained based on the two methods of theoretical solution and finite element simulation is drawn. The black solid line in the figure is the result of the theoretical solution, and the blue diamond point is the result of the finite element simulation. With the increase in the included angle, the momentum component transfer of the entire sound field along the z axis decreases continuously. Most of the radial components are converted into internal energy due to the mutual cancellation of symmetry, and the contribution to the ARF on the particles is very small. Therefore, the ARF received by the particles is mainly negatively correlated with the included angle. Yet/however, it is worth mentioning that, since the incident sound field is actually limited in

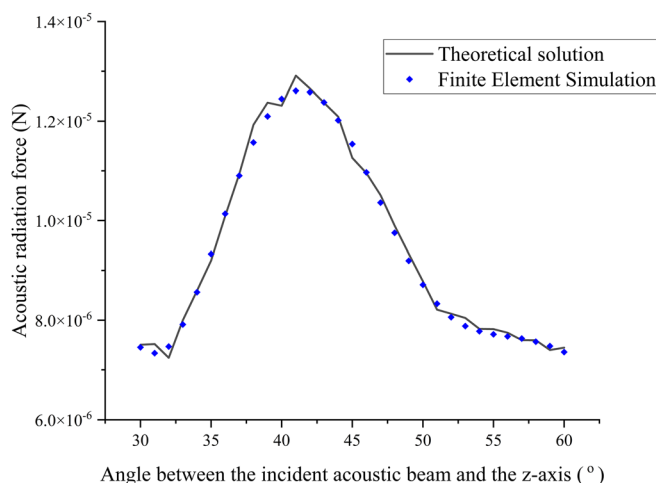


FIG. 5. (Color online) The ARF on the controlled spherical particle changing with the angle between the incident acoustic beam and the z axis.

width, the part of the sound field energy irradiated in front of the particle actually contributes very little to the ARF received by the particle. With the increase in the included angle, the proportion of the sound energy injected by the incident sound wave to the sound field behind the particle gradually increases. These two effects antagonize each other, making the ARF on the particle peaks around 40° .

C. The relationship between the ARF and the outer radius of the tube

Due to individual differences in the radius of the ureter, theoretical solutions based on the case of different outer tube radius are carried out. The tube thickness, the radius of the spherical particles, the angle between the incident beam and the z axis, and frequency of the incident beam are fixed at 0.25 mm, 0.74 mm, 45° , and 1 MHz, individually. As shown in Fig. 6, the ARF on spherical particles in the tube obtained based on the theoretical solution is drawn. It could be seen that there is one major peak at 1.08 mm and four minor peaks at 1.36, 1.44, 1.58, and 1.82 mm in Fig. 6. The maximum ARF is greater than 2×10^{-4} N. The peak position and peak size are reasonably predicted.

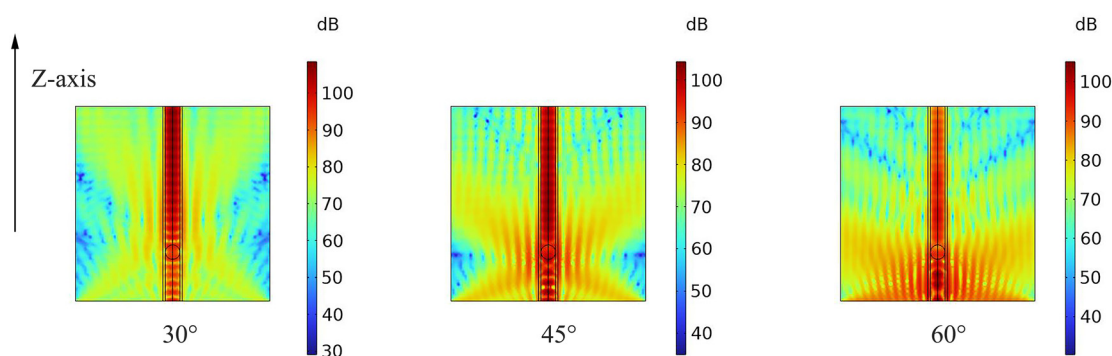


FIG. 4. (Color online) Sectional view of the sound pressure level distribution when the angle between the incident sound beam and the z axis is 30° , 45° , and 60° .

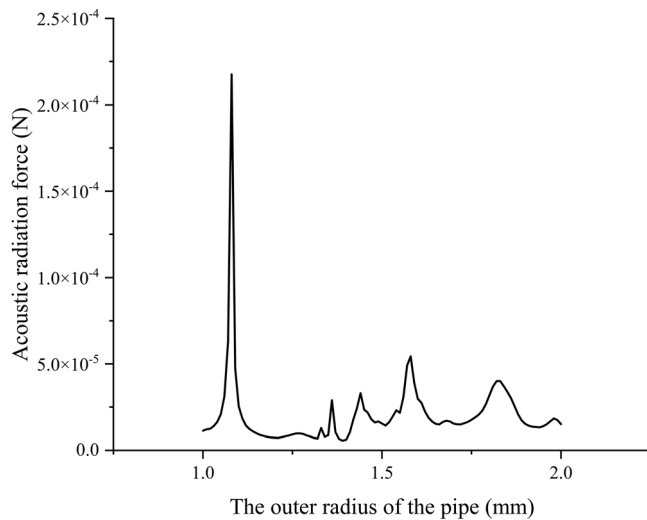


FIG. 6. The ARF on the controlled spherical particle changing with the outer radius of the tube.

D. The relationship between the ARF and the radius of the spherical particles

For the differences in the stone formation process, the radii of the calculus that need to be manipulated also vary. Therefore, theoretical solutions based on spherical particles of different radii are carried out. The tube thickness, the outer radius of the tube, the angle between the incident beam and the z axis, and frequency of the incident beam are fixed at 0.25 mm, 1 mm, 45° , and 1 MHz, individually. As shown in Fig. 7, the ARF on spherical particles in the tube obtained based on the theoretical solution is drawn. The peak obtained by two methods appears at $a = 0.58$ mm.

E. The relationship between the ARF and the viscosity coefficient of fluids

Due to differences in the concentration and composition of urine, diseases of the urinary system, for example, may cause proteinuria, resulting in large changes in urine viscosity.

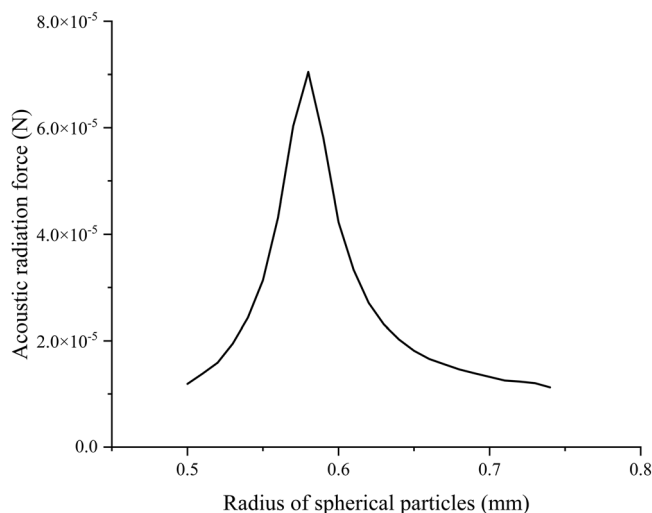


FIG. 7. The ARF on the controlled spherical particle changing with the radius of the spherical particle.

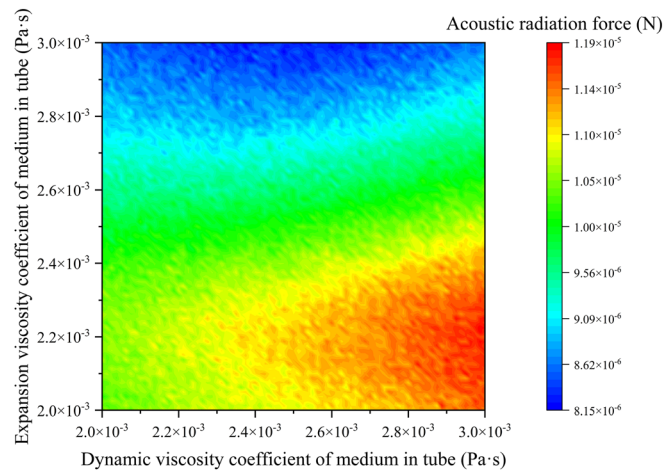


FIG. 8. (Color online) The ARF on the controlled spherical particle changing with the viscosity coefficient.

Therefore, it is necessary to calculate and predict the ARF in the case of different medium viscosities. Based on this, the ARFs experienced by spherical particles under different dynamic viscosity coefficient and expansion viscosity coefficient are plotted. As shown in Fig. 8, the ARF on particles under different viscosity conditions obtained by theoretical solution is plotted. Through this result, the urine viscosity of the patient can be tested, and corresponding recommendations can be made to increase the manipulation effect of the ARF on the calculus, such as drinking more or less water to change the concentration.

IV. CONCLUSION

This paper presents a scheme of the manipulation of particles in a tube based on the ARF. The analysis of sound field is carried out, and an analytical method for calculating the ARF on particles is proposed. The main parameters affecting the ARF on the particles are analyzed, which lays a foundation for the precise control of the ARF on the particles. Through the application scenario of promoting the expulsion of calculus in the ureter, finite element simulations are carried out. The feasibility and accuracy of the scheme are verified by comparing with the results of theoretical solution. This scheme has a wide range of application scenarios in the fields of life science, medicine, and industry and fills the gap of non-contact manipulation of particles in the tube based on ARF. Subsequently, the particles in the tube can be manipulated two-dimensionally through a rotationally asymmetric sound field, and more precise manipulation design can be carried out for more general environments, such as non-uniform tubes.

ACKNOWLEDGMENTS

This project was supported by National Key R&D Program of China Grant No. 2020YFA0211400, State Key Program of National Natural Science of China Grant No. 11834008, National Natural Science Foundation of China Grant No. 12174192, State Key Laboratory of Acoustics,

Chinese Academy of Science, Grant No. SKLA202210, and Key Laboratory of Underwater Acoustic Environment, Chinese Academy of Sciences, Grant No. SSHJ-KFKT-1701. The data that support the findings of this study are available from the corresponding author upon reasonable request.

APPENDIX

The specific expressions of each element in the scattering matrix in Eq. (20) are as follows:

$$\begin{aligned}
 a_{rn} &= nh_n^{(1)}(\alpha a) - \alpha r h_{n+1}^{(1)}(\alpha a), \\
 b_{rn} &= -n(n+1)h_n^{(1)}(\beta a), \\
 a'_{rn} &= k_L a j_{n+1}(k_L a) - n j_n(k_L a), \\
 b'_{rn} &= n(n+1)j_n(k_{2r} a), \\
 c_{rn} &= -I_n[n j_n(\alpha a) - \alpha r j_{n+1}(\alpha a)], \\
 a_m &= h_n^{(1)}(\alpha a), \\
 b_m &= -n(n+1)h_n^{(1)}(\beta a) + \beta r h_{n+1}^{(1)}(\beta a), \\
 a'_m &= -j_n(k_L a), \\
 b'_m &= n(n+1)j_n(k_{2r} a) + \beta r j_{n+1}(k_{2r} a), \\
 c_m &= -I_n j_n(\alpha a), \\
 A_{rn} &= \mu' \left[\left(n^2 - n - \frac{\beta^2 a^2}{2} \right) h_n^{(1)}(\alpha r) + 2\alpha a h_{n+1}^{(1)}(\alpha a) \right], \\
 B_{rn} &= \mu' \left[- (n-1)n(n+1)h_n^{(1)}(\beta a) \right. \\
 &\quad \left. + n(n+1)(\beta a)h_n^{(1)}(\beta a) \right], \\
 A'_{rn} &= \mu \left[\left(-n^2 + n + \left(1 + \frac{\lambda}{2\mu} \right) k_L^2 a^2 \right) j_n(k_L a) \right. \\
 &\quad \left. - (k_L a)j_{n+1}(k_L a) \right], \\
 B'_{rn} &= \mu \left[(n-1)n(n+1)j_n(k_{2r} a) \right. \\
 &\quad \left. - n(n+1)(k_{2r} a)j_{n+1}(k_{2r} a) \right], \\
 C_{rn} &= -\mu' A \left[\left(n^2 - n - \frac{\beta^2 a^2}{2} \right) j_n(\alpha a) + 2\alpha a j_{n+1}(\alpha a) \right], \\
 A_m &= \mu' \left[(n-1)h_n^{(1)}(\alpha a) - (\alpha a)h_{n+1}^{(1)}(\alpha a) \right], \\
 B_m &= \mu' \left[\left(-n^2 + 1 + \frac{\beta^2 a^2}{2} \right) h_n^{(1)}(\beta a) - (\beta a)h_{n+1}^{(1)}(\beta a) \right], \\
 A'_m &= \mu \left[-(n-1)j_n(k_L a) + (k_L a)j_{n+1}(k_L a) \right], \\
 B'_m &= \mu \left[- \left(-n^2 + 1 + \frac{k_{2r}^2 a^2}{2} \right) j_n(k_{2r} a) \right. \\
 &\quad \left. + (k_{2r} a)j_{n+1}(k_{2r} a) \right], \\
 C_m &= -\mu' I_n \left[(n-1)j_n(\alpha a) - (\alpha r)j_{n+1}(\alpha a) \right].
 \end{aligned}$$

- ¹A. Ashkin, "Forces of a single-beam gradient laser trap on a dielectric sphere in the ray optics regime," *Biophys. J.* **61**, 569–582 (1992).
- ²Z. X. Gong and M. Baudoin, "Equivalence between angular spectrum-based and multipole expansion-based formulas of the acoustic radiation force and torque," *J. Acoust. Soc. Am.* **149**, 3469–3482 (2021).
- ³S. Sepehrirahnama, S. Oberst, Y. K. Chiang, and D. Powell, "Acoustic radiation force and radiation torque beyond particles: Effects of nonspherical shape and Willis coupling," *Phys. Rev. E* **104**, 065003 (2021).
- ⁴Q. Wang, A. Riaud, J. Zhou, Z. X. Gong, and M. Baudoin, "Acoustic radiation force on small spheres due to transient acoustic fields," *Phys. Rev. Appl.* **15**, 044034 (2021).
- ⁵D. Baresch, J. L. Thomas, and R. Marchiano, "Observation of a single-beam gradient force acoustical trap for elastic particles: Acoustical tweezers," *Phys. Rev. Lett.* **116**, 024301 (2016).
- ⁶X. D. Fan and L. K. Zhang, "Phase shift approach for engineering desired radiation force: Acoustic pulling force example," *J. Acoust. Soc. Am.* **150**, 102–110 (2021).
- ⁷Z. X. Gong, P. L. Marston, W. Li, and Y. B. Chai, "Multipole expansion of acoustical Bessel beams with arbitrary order and location," *J. Acoust. Soc. Am.* **141**, EL574–EL578 (2017).
- ⁸P. L. Marston, "Axial radiation force of a Bessel beam on a sphere and direction reversal of the force," *J. Acoust. Soc. Am.* **120**, 3518–3524 (2006).
- ⁹P. L. Marston, "Negative axial radiation forces on solid spheres and shells in a Bessel beam (L)," *J. Acoust. Soc. Am.* **122**, 3162–3165 (2007).
- ¹⁰P. L. Marston, "Radiation force of a helicoidal Bessel beam on a sphere," *J. Acoust. Soc. Am.* **125**, 3539–3547 (2009).
- ¹¹P. L. Marston, "Comment on 'Radiation forces and torque on a rigid elliptical cylinder in acoustical plane progressive and (quasi)standing waves with arbitrary incidence' [Phys. Fluids. **28**, 077104 (2016)]," *Phys. Fluids* **29**, 029101 (2017).
- ¹²F. G. Mitri, "Radiation forces and torque on a rigid elliptical cylinder in acoustical plane progressive and (quasi)standing waves with arbitrary incidence," *Phys. Fluids* **28**, 077104 (2016).
- ¹³Y. P. Qiao, X. W. Zhang, M. Y. Gong, H. B. Wang, and X. Z. Liu, "Acoustic radiation force and motion of a free cylinder in a viscous fluid with a boundary defined by a plane wave incident at an arbitrary angle," *J. Appl. Phys.* **128**, 044902 (2020).
- ¹⁴O. A. Sapozhnikov and M. R. Bailey, "Radiation force of an arbitrary acoustic beam on an elastic sphere in a fluid," *J. Acoust. Soc. Am.* **133**, 661–676 (2013).
- ¹⁵H. B. Wang, S. Gao, Y. P. Qiao, J. H. Liu, and X. Z. Liu, "Theoretical study of acoustic radiation force and torque on a pair of polymer cylindrical particles in two Airy beams fields," *Phys. Fluids* **31**, 047103 (2019).
- ¹⁶R. R. Wu, K. X. Cheng, X. Z. Liu, J. H. Liu, X. F. Gong, and Y. F. Li, "Study of axial acoustic radiation force on a sphere in a Gaussian quasi-standing field," *Wave Motion* **62**, 63–74 (2016).
- ¹⁷R. R. Wu, K. X. Cheng, X. Z. Liu, J. H. Liu, Y. W. Mao, and X. F. Gong, "Acoustic radiation force on a double-layer microsphere by a Gaussian focused beam," *J. Appl. Phys.* **116**, 144903 (2014).
- ¹⁸L. K. Zhang and P. L. Marston, "Acoustic radiation force expressed using complex phase shifts and momentum-transfer cross sections," *J. Acoust. Soc. Am.* **140**, EL178–EL183 (2016).
- ¹⁹L. K. Zhang and P. L. Marston, "Axial radiation force exerted by general non-diffracting beams," *J. Acoust. Soc. Am.* **131**, EL329–EL335 (2012).
- ²⁰Y. P. Qiao, M. Gong, H. Wang, J. Lan, T. Liu, J. Liu, Y. Mao, A. He, and X. Liu, "Acoustic radiation force on a free elastic sphere in a viscous fluid: Theory and experiments," *Phys. Fluids* **33**, 047107 (2021).
- ²¹M. Y. Gong, Y. Qiao, Z. Fei, Y. Li, J. Liu, Y. Mao, A. He, and X. Liu, "Non-diffractive acoustic beams produce negative radiation force in certain regions," *AIP Adv.* **11**, 065029 (2021).
- ²²M. Y. Gong, Y. P. Qiao, J. Lan, and X. Z. Liu, "Far-field particle manipulation scheme based on X wave," *Phys. Fluids* **32**, 117104 (2020).
- ²³P. L. Marston and L. K. Zhang, "Unphysical consequences of negative absorbed power in linear passive scattering: Implications for

- radiation force and torque,” *J. Acoust. Soc. Am.* **139**, 3139–3144 (2016).
- ²⁴P. L. Marston and L. K. Zhang, “Relationship of scattering phase shifts to special radiation force conditions for spheres in axisymmetric wavefields,” *J. Acoust. Soc. Am.* **141**, 3042–3049 (2017).
- ²⁵J. Y. Shi, X. F. Zhang, R. M. Chen, and G. B. Zhang, “Acoustic radiation force of a solid elastic sphere immersed in a cylindrical cavity filled with ideal fluid,” *Wave Motion* **80**, 37–46 (2018).
- ²⁶T. Baasch, A. Pavlic, and J. Dual, “Acoustic radiation force acting on a heavy particle in a standing wave can be dominated by the acoustic microstreaming,” *Phys. Rev. E* **100**, 061102 (2019).
- ²⁷I. D. Toftul, K. Y. Bliokh, M. I. Petrov, and F. Nori, “Acoustic radiation force and torque on small particles as measures of the canonical momentum and spin densities,” *Phys. Rev. Lett.* **123**, 183901 (2019).
- ²⁸M. A. Ghanem, A. D. Maxwell, Y.-N. Wang, B. W. Cunitz, V. A. Khokhlova, O. A. Sapozhnikov, and M. R. Bailey, “Noninvasive acoustic manipulation of objects in a living body,” *Proc. Natl. Acad. Sci. U.S.A.* **117**, 16848–16855 (2020).
- ²⁹M. Baudoin, J.-L. Thomas, R. Al Sahely, J.-C. Gerbedoen, Z. Gong, A. Sivery, O. B. Matar, N. Smagin, P. Favreau, and A. Vlandas, “Spatially selective manipulation of cells with single-beam acoustical tweezers,” *Nat. Commun.* **11**, 4244 (2020).